ISSN: 2689-1204

Review article

Journal of Applied Material Science & Engineering Research

Solving Partial Derivation Equations in Detail in Double-Rotor Flux Switching Permanent Magnet with H-Shape Stator Machines to Obtain Magnetic Flux Density

Ehsan Shirzad*

Department of Electrical and Electronic Engineering, University of Bojnord, Bojnord, I. R. of Iran

***Corresponding Author**

Ehsan Shirzad, Department of Electrical and Electronic Engineering, University of Bojnord, Bojnord, I. R. of Iran

Submitted: 2023, Oct 23; **Accepted:** 2023, Nov 27; **Published:** 2023, Dec 05

Citation: Shirzad, E. (2023). Solving Partial Derivation Equations in Detail in Double-Rotor Flux Switching Permanent Magnet with H-Shape Stator Machines to Obtain Magnetic Flux Density. *J App Mat Sci & Engg Res, 7*(2), 182-195.

Abstract

In this paper, aim is turning double-rotor flux switching permanent magnet with H-shape stator machine (DRFSPMWHSSMs) into mathematical equations via Maxwell relations to provide a 3-quasi model for calculating flux density at arbitrary point of DRFSPMWHSSMs. Remarkable reason for opting this type of machine is 2 rotors can be energized only by integrated stator that is an obstacle against squandering core loss. Merging reluctance and permanent magnet machine into a configuration has high advantages like receiving appropriate power density in low volume of geometric structure. The model implemented in this article can be answerable for the entire distinct mentioned machine with the different number of teethes. After extracting equations, comparison between numerical method and this analytical model for efficacy of analytical model is done.

Keywords: Partial Derivation Equation, 3-Quasi Analytical Model, Numerical Model, Subdomain, Boundary Conditions, Hybrid Electrical Vehicle.

Nomenclature

$\boldsymbol{A}$	Magnetic vector potential (V.s/m)	r	Radial direction
$\boldsymbol{B}$	Magnetic flux density vector (T)	θ	Tangential direction
B_r	Radial component of $\boldsymbol{B}$ (T)	z	Axial direction
$\boldsymbol{B_\theta}$	Tangential component of $\boldsymbol{B}$ (T)	*iry*	Inner rotor yoke
$\boldsymbol{H}$	Magnetic field intensity vector (A/m)	*irs*	Inner rotor slot
$\boldsymbol{J}$	Armature current density vector (A/m^2)	*ia*	Inner airgap
μ_0	Free space permeability (H/m).	*iss*	Inner stator slot
μ_r	Relative permeability	*isy*	Inner stator yoke
N_{iss}	Number of inner stator slots	*osy*	Outer stator yoke
N_{irs}	Number of inner rotor slots	*oss*	Outer stator slot
N_{oss}	Number of outer stator slots	*oa*	Outer airgap
N_{ors}	Number of outer rotor slots	*ors*	Outer rotor slot
α_i	Central angle of *i*th slot of inner rotor	*ory*	Outer rotor yoke
β_i	Central angle of *i*th slot of inner stator	υ	Angular displacement of rotor
σ_i	Central angle of *i*th slot of outer rotor	*m, n, v, k*	Harmonic order
ψ_i	Central angle of *i*th slot of outer stator	*a, b, c, d, e*	Unknown coefficient
Γ_i	Central angle of *i*th slot of permanent magnet		
δ	Width of slots of inner rotor		
γ	Width of slots of inner stator		
β	Width of permanent magnets		

1. Introduction

The permanent magnet flux-switching (PMFS) machines are suitable machine due to their sinusoidal phase back-EMF waveform, high torque density, and robust, simple rotor structure [1-4]. They are also very suitable for outer-rotor application [5-8]. PMSMs can be categorized into rotor-PM machines and stator-PM machines. Totally, the rotor-PM machines, like surface-mounted, surface inset, and interior types, are too good in current domestic and industrial applications because of recognized their features. Newly, the switched flux PM machines (SFPMMs), have introduced to overcome some of the problems suffered from rotor-PM machines despite some of their drawbacks such as a reduction of slot space and a relatively high working frequency [9]. Accordingly, the most researches are on stator-based and rotor-based PM machines either separately or by comparison [10-12]. Many new structures of PMSMs with high torque density have been proposed, Furthermore, PM machines, in particular, fractional slot PM machines and SFPMMs, heavily researched recently, are often equipped with concentrated windings offering the advantage of short end turns for reduced winding cost, weight, and loss, but suffering a low effective winding factor. Hence, research and development of high performance electric machines with less or no rare earth magnets is of continuously great importance. In comparison to the induction machines and switched reluctance machines, ferrite PM machines are attracted for the rare earth magnet machines although low torque of ferrite PM machines is not satisfying [13-14]. To overcome this issue, electrical machines with two airgap and spoke-type structure have been found to increase torque and power density [15-16].Flux switching permanent magnet (FSPM) are favorite choice due to large torque capability, sinusoidal back-electromotive force (EMF) waveforms, high torque (power) density, as well as compact and robust structure since both energy supply are on stator [17,31-37]. There are some studies reported in literatures dealing with analytical and numerical magnetic field calculations of FSPM. In a prototype of a high-power three-phase 12-stator-slot/10-rotor-pole FSPM motor for hybrid electric vehicles (HEVs) is designed by FEM [38]. In a new flux switching permanent magnet machine (S-FSPM) with an outer-rotor configuration is investigated by theoretical analysis and two-dimensional (2-D) FEM [39]. Kim et al. have presented a new study on the comparison of dual-rotor single-stator (DRSS) and dual-stator single-rotor (DSSR) axial flux-switching permanent magnet machines by 3-D finite element analysis (FEA) and experimental verification [40]. Ina 2-D analytical method is investigated for FSPM by using Maxwell equations [41,42]. Yu et al. have proposed a double-stator flux switched permanent magnet motor (DSFSM) adopting stator-partitioned structure with double air gaps; the DSFSM is designed and verified by FEM [43]. Yang et al. have presented a simple analytical model for switched flux memory machines to provide in-depth insight into its working mechanism [44-50].

The contribution of the proposed analytical model is as follows:
• The 2D analytical model based on the Maxwell equations for double-mechanical port FSPMMs has been presented for the first time.
• The proposed model is able to incorporate the influences of the inner and outer parts on each other.

2. Structure of Investigated Machine

Studied machine is composed of inner and outer rotors are lack of winding, stator and permanent magnets mounted on teethes of stator that in figure 1 is shown cross section of this structure and in figure 2 three dimensional geometric is illustrated. Permanent magnets on stator magnetize in direction of tangential alone that permanent magnets in adjacent to each other are in opposite magnetization direction also, stator is H-shape formation that slots in stator can be acceptable for two groups of winding to generate energy for rotation of rotors.

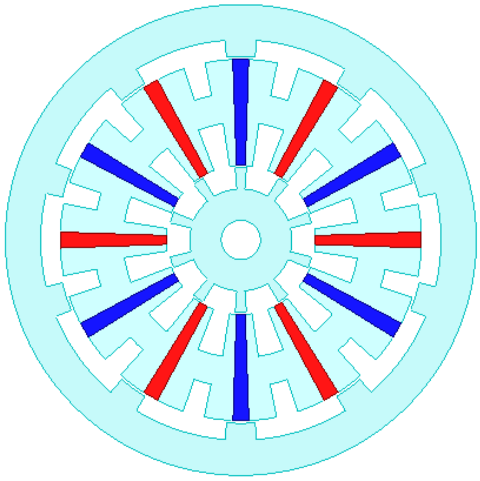

Figure 1: Two dimensional of DRFSPMWHSSMs

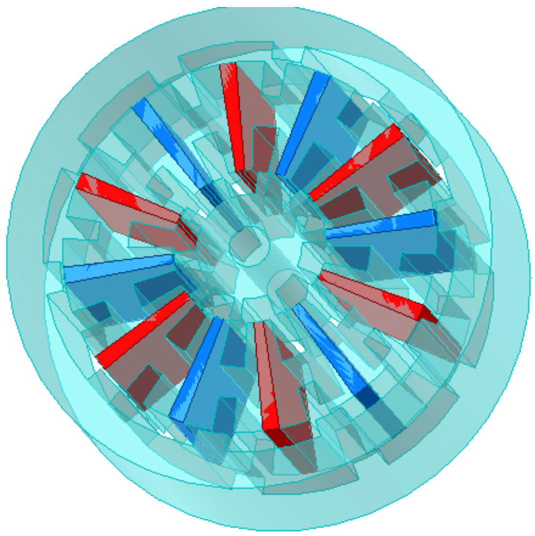

Figure 2: Three dimensional of DRFSPMWHSSMs

3. Procedure of Three-Phase Winding

The prototype machine investigating has determined layout of winding based on table 1 and table 2 for single and double layer winding, the number of slots for stator is 12 and for two rotors are 10. Energizing into wires of winding is balanced to produce less-ripple torque and without spike which current for three phases is in accordance with relations1, 2 and 3 that I_m andω_eare respectively magnitude of current and electrical angular velocity.

$$\mathrm{i_a(t) = sin(t)} \quad (1)$$

$$i_b(t) = I_m \sin(\omega_e t - \frac{2\pi}{3}) \quad (2)$$

$$i_c(t) = I_m \sin(\omega_e t + \frac{2\pi}{3}) \quad (3)$$

Number of slot	Layout
1	A+
2	C-
3	C-
4	B+
5	B+
6	A-
7	A-
8	C+
9	C+
10	B-
11	B-
12	A+

Table 1. Layout of single-layer winding

Number of slot	Right side	Left side
1	A-	B+
2	B-	C+
3	C-	A+
4	A-	B+
5	B-	C+
6	C-	A+
7	A-	B+
8	B-	C+
9	C-	A+
10	A-	B+
11	B-	C+
12	C-	A+

Table 2. Layout of 2-layer winding

4. Fundamental Equations

Assumptions to simplify problem is imminent that some reasoning to solve and model are as follows:

- Direction of magnetic potential vector and current density vector is in depth and z
- Length in direction of z is infinite
- Permeability for cores is infinite
- Eddy current is eliminated
- End-effect is neglected

Based on the assumptions given above, the Maxwell equation for a sub-region having both current density and PMs is expressed as follows:

$$-\nabla^2 A_z^i = \mu_0 \mu_r J_z^i + \frac{\mu_0}{r}\left(\frac{\partial M_r}{\partial \theta} - r\frac{\partial M_\theta}{\partial r}\right) \quad (4)$$

It is noted that in the PM sub-regions J_z=0, and in the winding sub-regions $M_r = M_\theta$ =0. For other sub-regions both *J* and *M* are zero, as shown in the following expression:

$$-\frac{1}{r^2}\frac{\partial^2 A_z^i}{\partial \theta^2} - \frac{1}{r}\frac{\partial}{\partial r}(r\frac{\partial A_z^i}{\partial r}) = 0 \quad (5)$$

The magnetic flux density components are obtained for each sub-region by using curl from the magnetic vector potential, i.e. **B=∇×A**, and the magnetic field intensity is calculated by (6).

$$\boldsymbol{H} = \frac{\boldsymbol{B}}{\mu_0 \mu_r} \quad (6)$$

Based on relations (4), (5) and B=∇×A, magnetic potential vector and magnetic flux density are obtained as follows:

4.1 Slots of Inner Rotor

$$A^{z}_{IRS}(r,\theta) = c_{0j} + \sum_{m=1}^{\infty}\left(c_{1mj} r^{\frac{m\pi}{\delta}} + c_{1mj} R_{ryi}^{2\frac{m\pi}{\delta}} r^{-\frac{m\pi}{\delta}}\right)\cos\left(\frac{m\pi}{\delta}\left(\theta - \alpha_j - \vartheta + \frac{\delta}{2}\right)\right) \quad (7)$$

$$B^{r}_{IRS}(r,\theta) = -\frac{m\pi}{\delta}\sum_{m=1}^{\infty}\left(c_{1mj} r^{\frac{m\pi}{\delta}-1} + c_{1mj} R_{ryi}^{2\frac{m\pi}{\delta}} r^{-\frac{m\pi}{\delta}-1}\right)\sin\left(\frac{m\pi}{\delta}\left(\theta - \alpha_j - \vartheta + \frac{\delta}{2}\right)\right) \quad (8)$$

$$B_{IRS}^{\theta}(r,\theta) = \frac{-m\pi}{\delta}\sum_{m=1}^{\infty} c_{1jm}\left(r^{\frac{m\pi}{\delta}-1} - R_{ryi}^{\frac{2m\pi}{\delta}} r^{\frac{-m\pi}{\delta}-1}\right)\cos\left(\frac{m\pi}{\delta}\left(\theta - \alpha_j - \vartheta + \frac{\delta}{2}\right)\right) \quad (9)$$

4.2 Slots of Outer Rotor

$$A^{z}_{ORS}(r,\theta) = c'_{0j} + \sum_{m'=1}^{\infty}\left(c'_{1m'j} r^{\frac{m'\pi}{\delta'}} + c'_{1m'j} R_{ryo}^{2\frac{m'\pi}{\delta'}} r^{-\frac{m'\pi}{\delta'}}\right)\cos\left(\frac{m'\pi}{\delta'}\left(\theta - \alpha_j' - \vartheta' + \frac{\delta'}{2}\right)\right) \quad (10)$$

$$B^{r}_{ORS}(r,\theta) = -\frac{m'\pi}{\delta'}\sum_{m'=1}^{\infty}\left(c'_{1m'j} r^{\frac{m'\pi}{\delta'}-1} + c'_{1m'j} R_{ryo}^{2\frac{m'\pi}{\delta'}} r^{-\frac{m'\pi}{\delta'}-1}\right)\sin\left(\frac{m'\pi}{\delta'}\left(\theta - \alpha'_j - \vartheta' + \frac{\delta'}{2}\right)\right) \quad (11)$$

$$B_{ORS}^{\theta}(r,\theta) = \frac{-m'\pi}{\delta'}\sum_{m'=1}^{\infty} c'_{1m'j}\left(r^{\frac{m'\pi}{\delta'}-1} - R_{ryo}^{\frac{2m'\pi}{\delta'}} r^{\frac{-m'\pi}{\delta'}-1}\right)\cos\left(\frac{m'\pi}{\delta'}\left(\theta - \alpha'_j - \vartheta' + \frac{\delta'}{2}\right)\right) \quad (12)$$

4.3 Inner Airgap

$$A^{z}_{IAG}(r,\theta) = \sum_{n=1}^{\infty}\left(a_{1n} r^{n} + a_{2n} r^{-n}\right)\sin(n\theta) + \left(b_{1n} r^{n} + b_{2n} r^{-n}\right)\cos(n\theta) \quad (13)$$

$$B_{IAG}^{r}(r,\theta) = n\sum_{n=1}^{\infty}\left(a_{1n} r^{n-1} + a_{2n} r^{-n-1}\right)\cos(n\theta) - \left(b_{1n} r^{n-1} + b_{2n} r^{-n-1}\right)\sin(n\theta) \quad (14)$$

$$B^{\theta}_{IAG}(r,\theta) = \sum_{n=1}^{\infty} -\left(na_{1n} r^{n-1} - na_{2n} r^{-n-1}\right)\sin(n\theta) - \left(nb_{1n} r^{n-1} - nb_{2n} r^{-n-1}\right)\cos(n\theta) \quad (15)$$

4.4Outer Airgap

$$A^{\theta}_{OAG}(r,\theta) = \sum_{n=1}^{\infty}\left(a'_{1n} r^{n} + a'_{2n} r^{-n}\right)\sin(n\theta) + \left(b'_{1n} r^{n} + b'_{2n} r^{-n}\right)\cos(n\theta) \quad (16)$$

$$B_{OAG}^{r}(r,\theta) = n\sum_{n=1}^{\infty}\left(a'_{1n} r^{n-1} + a'_{2n} r^{-n-1}\right)\cos(n\theta) - \left(b'_{1n} r^{n-1} + b'_{2n} r^{-n-1}\right)\sin(n\theta) \quad (17)$$

$$B^{\theta}_{OAG}(r,\theta) = \sum_{n=1}^{\infty} -\left(na'_{1n} r^{n-1} - na'_{2n} r^{-n-1}\right)\sin(n\theta) - \left(nb'_{1n} r^{n-1} - nb'_{2n} r^{-n-1}\right)\cos(n\theta) \quad (18)$$

4.5 Permanent Magnet

$$A_{IPM}{}^{z}(r,\theta) = e_0 + u_0 M_j R_{pmi}\ln(r) - u_0 M_j r + \sum_{v=1}^{\infty}\left(e_{1vj}\, r^{\frac{v\pi}{\beta}} + e_{1vj} R_{pmi}^{\frac{2v\pi}{\beta}} r^{\frac{-v\pi}{\beta}}\right)\cos\left(\frac{\pi v}{\beta}\left(\theta - \Gamma_j + \frac{\beta}{2}\right)\right) \quad (19)$$

$$B_{IPM}{}^{r}(r,\theta) = \sum_{v=1}^{\infty} -\frac{\pi v}{\beta}\left(e_{1vj}\, r^{\frac{v\pi}{\beta}-1} + e_{1vj} R_{pmi}^{\frac{2v\pi}{\beta}} r^{\frac{-v\pi}{\beta}-1}\right)\sin\left(\frac{\pi v}{\beta}\left(\theta - \Gamma_j + \frac{\beta}{2}\right)\right) \quad (20)$$

$$B_{IPM}{}^{\theta}(r,\theta) = u_0 M_j\left(-\frac{R_{pmi}}{r} + 1\right) - \frac{v\pi}{\beta}\sum_{v=1}^{\infty} e_{1jv}\left(r^{\frac{v\pi}{\beta}-1} - R_{pmi}^{\frac{2v\pi}{\beta}} r^{\frac{-v\pi}{\beta}-1}\right)\cos\left(\frac{v\pi}{\beta}\left(\theta - \Gamma_j + \frac{\beta}{2}\right)\right) \quad (21)$$

4.6 Inner Stator Slot

$$A^{z}{}_{IW}(r,\theta) = d_0 + \frac{1}{2}u_0 J_0 R_{yi}{}^{2}\ln(r) - \frac{1}{4}u_0 J_0 r^2 + \sum_{k=1}^{\infty}\left(\frac{u_0 J_{jk} r^2}{\left(\frac{k\pi}{\gamma}\right)^2 - 4} + d_{1kj} r^{\left(\frac{k\pi}{\gamma}\right)} + \left(\frac{2u_0 J_{jk}\frac{R_{yi}}{\left(\frac{k\pi}{\gamma}\right)^2 - 4} + \frac{k\pi}{\gamma} d_{1kj} R_{yi}^{\frac{k\pi}{\gamma}-1}}{k\frac{\pi}{\gamma} R_{yi}^{-\frac{k\pi}{\gamma}-1}}\right) r^{\left(-\frac{k\pi}{\gamma}\right)}\right)\cos\left(\frac{k\pi}{\gamma}\left(\theta - \lambda_j + \frac{\gamma}{2}\right)\right) \quad (22)$$

$$B^{r}{}_{IW}(r,\theta) = \sum_{k=1}^{\infty} -\frac{k\pi}{\gamma}\left(\frac{u_0 J_{jk} r}{\left(\frac{k\pi}{\gamma}\right)^2 - 4} + d_{1kj} r^{\left(\frac{k\pi}{\gamma}\right)-1} + \left(\frac{2u_0 J_{jk}\frac{R_{yi}}{\left(\frac{k\pi}{\gamma}\right)^2 - 4} + \frac{k\pi}{\gamma} d_{1kj} R_{yi}^{\frac{k\pi}{\gamma}-1}}{k\frac{\pi}{\gamma} R_{yi}^{\frac{-k\pi}{\gamma}-1}}\right) r^{\left(-\frac{k\pi}{\gamma}\right)-1}\right)\sin\left(\frac{k\pi}{\gamma}\left(\theta - \lambda_j + \frac{\gamma}{2}\right)\right) \quad (23)$$

(24)

$$B_{IW}^{\theta}(r,\theta) = -\frac{1}{2}\frac{u_0 J_0 R_{yi}^{2}}{r} + \frac{1}{2}u_0 J_0 r - \sum_{k=1}^{\infty}\left(\frac{2u_0 J_{jk} r}{\left(\frac{k\pi}{\gamma}\right)^2 - 4} + \left(\frac{k\pi}{\gamma}\right) d_{1kj} r^{\left(\frac{k\pi}{\gamma}\right)-1} - \left(\frac{k\pi}{\gamma}\right)\left(\frac{2u_0 J_{jk}\frac{R_{yi}}{\left(\frac{k\pi}{\gamma}\right)^2 - 4} + \frac{k\pi}{\gamma} d_{1kj} R_{yi}^{\frac{k\pi}{\gamma}-1}}{k\frac{\pi}{\gamma} R_{yi}^{\frac{-k\pi}{\gamma}-1}}\right) r^{\left(-\frac{k\pi}{\gamma}\right)-1}\right)\cos\left(\frac{k\pi}{\gamma}\left(\theta - \lambda_j + \frac{\gamma}{2}\right)\right)$$

4.7 Outer Stator Slot

(22)

$$A^{z}_{OW}(r,\theta) = d`0` + \frac{1}{2}u_0 J_0 R_{yo}^{2}\ln(r) - \frac{1}{4}u_0 J_0 r^2 + \sum_{k=1}^{\infty}\left(\frac{u_0 J_{jk} r^2}{\left(\frac{k\pi}{\gamma'}\right)^2 - 4} + d_{1k'j} r^{\left(\frac{k'\pi}{\gamma'}\right)} + \left(\frac{2u_0 J_{jk'}\frac{R_{yo}}{\left(\frac{k'\pi}{\gamma'}\right)^2 - 4} + \frac{k'\pi}{\gamma'} d`1k'j` R_{yo}^{\frac{k'\pi}{\gamma'}-1}}{k'\frac{\pi}{\gamma'} R_{yo}^{\frac{-k'\pi}{\gamma'}-1}}\right) r^{\left(-\frac{k'\pi}{\gamma'}\right)}\right)\cos\left(\frac{k'\pi}{\gamma'}\left(\theta - \lambda`j` + \frac{\gamma'}{2}\right)\right)$$

(23)

$$B^{r}_{OW}(r,\theta) = \sum_{k'=1}^{\infty} - \frac{k'\pi}{\gamma'}\left(\frac{u_0 J_{jk'} r}{\left(\frac{k'\pi}{\gamma'}\right)^2 - 4} + d'_{1k'j} r^{\left(\frac{k'\pi}{\gamma'}\right)-1} + \left(\frac{2u_0 J_{jk'}\frac{R_{yo}}{\left(\frac{k'\pi}{\gamma'}\right)^2 - 4} + \frac{k'\pi}{\gamma'} d'_{1k'j} R_{yo}^{\frac{k'\pi}{\gamma'}-1}}{k'\frac{\pi}{\gamma'} R_{yi}^{-\frac{k'\pi}{\gamma'}-1}}\right) r^{\left(-\frac{k'\pi}{\gamma'}\right)-1}\right)\sin\left(\frac{k'\pi}{\gamma'}\left(\theta - \lambda'_j + \frac{\gamma'}{2}\right)\right)$$

$$B_{OW}^{\theta}(r,\theta) = -\frac{1}{2}\frac{u_0 J_0 R_{yo}^{2}}{r} + \frac{1}{2}u_0 J_0 r - \sum_{k'=1}^{\infty}\left(\frac{2u_0 J_{jk'} r}{\left(\frac{k'\pi}{\gamma'}\right)^2 - 4} + \left(\frac{k'\pi}{\gamma'}\right) d'_{1k'j}\, r^{\left(\frac{k'\pi}{\gamma'}\right)-1} - \left(\frac{k'\pi}{\gamma'}\right)\left(\frac{2u_0 J_{jk'}\frac{R_{yo}}{\left(\frac{k'\pi}{\gamma'}\right)^2 - 4} + \frac{k'\pi}{\gamma'} d_{1k'j} R_{yo}^{\frac{k'\pi}{\gamma'}-1}}{\frac{k'\pi}{\gamma'} R_{yo}^{\frac{-k'\pi}{\gamma'}-1}}\right) r^{\left(\frac{-k'\pi}{\gamma'}\right)-1}\right)\cos\left(\frac{k'\pi}{\gamma'}\left(\theta - \lambda'_j + \frac{\gamma'}{2}\right)\right) \tag{24}$$

Unknown coefficients are obtained by boundary conditions that magnetic potential vector and radial flux intensity are continuous between each adjacent regionshown in appendix.

5. Results

Relations from (1) to (24) contribute to achieve magnetic flux density in directions of radial and tangential for both single layer and double layer winding in inner and outer airgap for DRFSPMWHSSMs. To confirm outputs brought from partial derivation equations, comparison between FEM and analytical model is as an observer to verify that then a case study based on table 1 is determined to cast the geometric of DRFSPMWHSSMs.

Parameters	Value
Number of inner phases, N_{iph}	3
Number of outer phases, N_{oph}	3
Number of inner rotor slots, N_{irs}	10
Number of outer rotor slots, N_{ors}	10
Number of inner stator slots, N_{iss}	12
Number of outer stator slots, N_{oss}	12
Number of conductors per each inner slot	40
Number of conductors per each outer slot	20
Relative permeability of PM, μ_{rpm}	1
Residual flux density, B_{rem}	1.2T
Maximum current for inner winding, I_{maxi}	20A
Maximum current for inner winding, I_{maxo}	20A
Maximum current density of inner winding, J_i	$6A/mm^2$
Maximum current density of outer winding, J_o	$6A/mm^2$
Inner rotor yoke radius, R_{ryi}	26mm
Outer rotor yoke radius, R_{ryo}	102mm
Inner stator yoke radius, R_{yi}	60mm
Outer stator yoke radius, R_{yo}	75mm
Inner radius of inner stator, R_{si}	38mm
Outer radius of outer stator, R_{so}	92.09mm
Inner radius of outer rotor, R_{ro}	96mm
Outer radius of inner rotor, R_{ri}	35mm
Inner radius of permanent magnet, R_{pmi}	63.63mm
Outer radius of permanent magnet, R_{pmo}	72.67mm
Width of inner rotor slot, w_{ri}	26.99 π/180 rad
Width of outer rotor slot, w_{ro}	27.01π/180 rad
Width of inner stator slot, w_{si}	12.5 π/180 rad
Width of outer stator slot, w_{so}	6.92 π/180 rad
Width of PM, w_{pmi}	3.24 π/180 rad
Stack length, L_s	100mm

Table.3 Specification ofDRFSPMWHSSMs

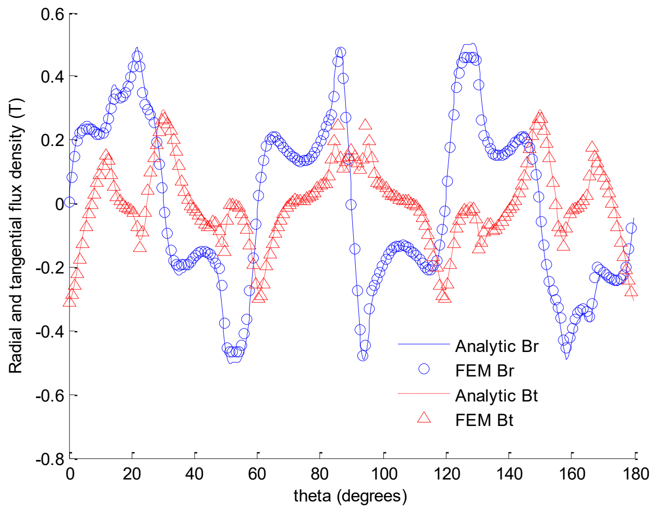

Figure 3: Radial and tangential flux density for inner part (r =35.6mm) for only permanent magnet

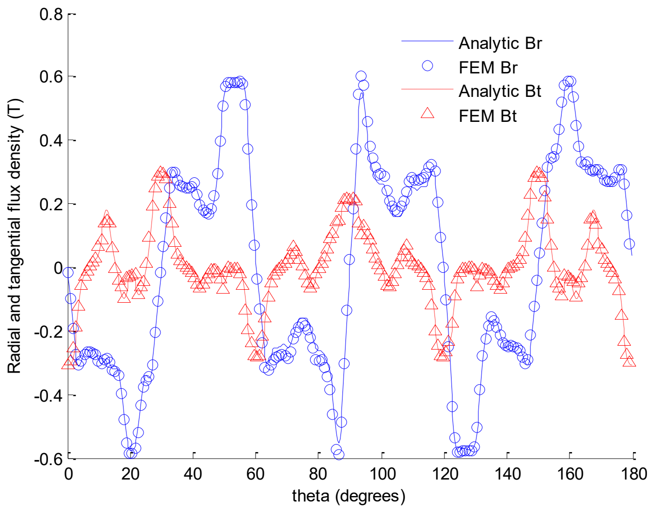

Figure 4: Radial and tangential flux density for outer part (r =94mm)for only permanent magnet

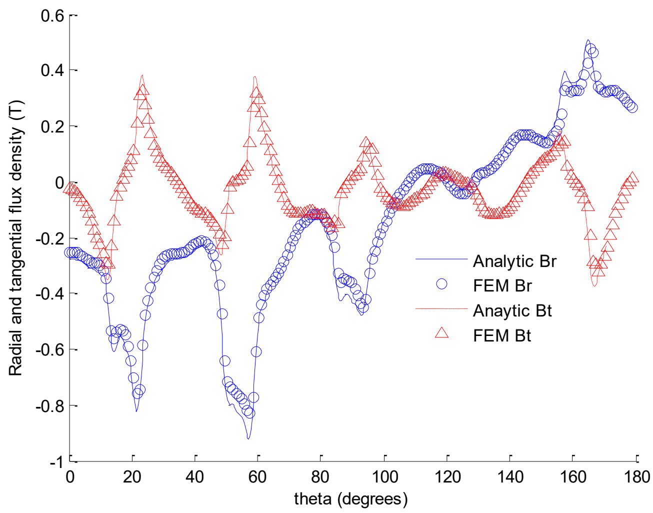

Figure5. Radial and tangential flux density for inner part (r =35.6mm&t=0) for only single layer winding

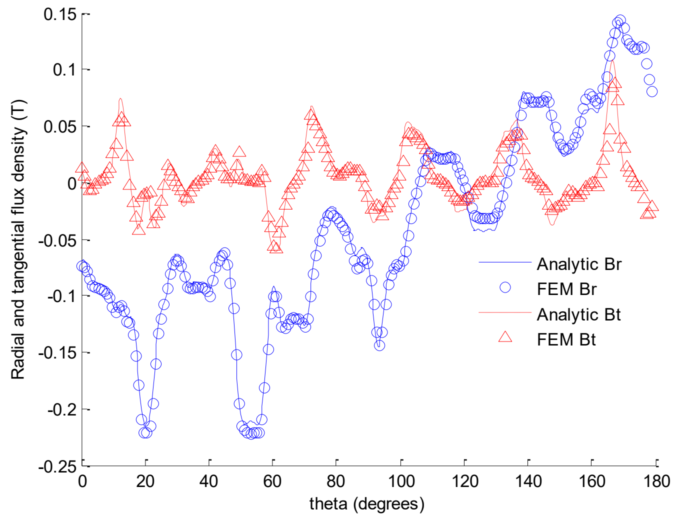

Figure 6: Radial and tangential flux density for outer part (r =94mm&t=0) for only single layer winding

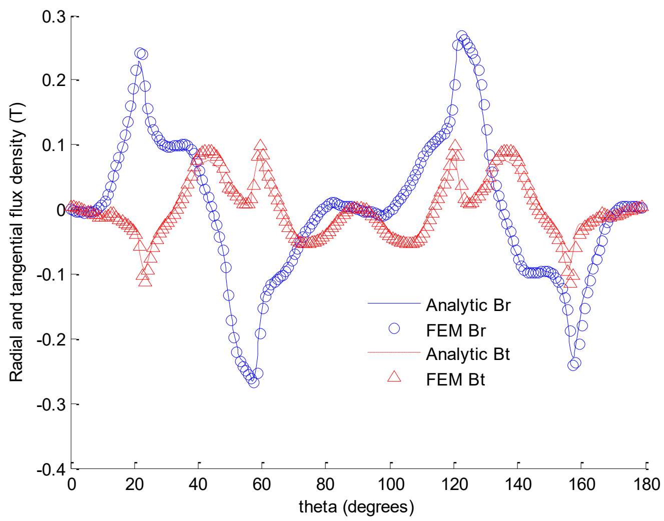

Figure 7: Radial and tangential flux density for outer part (r =35.6mm&t=0) for only double layer winding

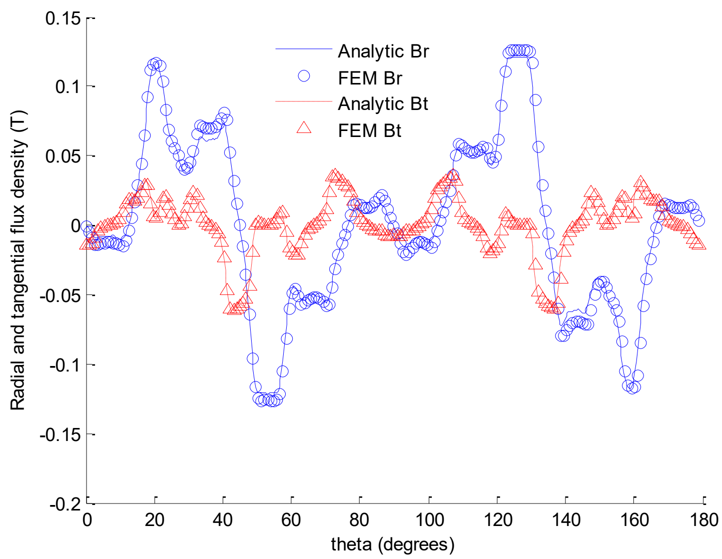

Figure 8: Radial and tangential flux density for outer part (r =94mm&t=0) for only double layer winding

6. Conclusions

In this paper, a flawless model for designing DRFSPMWHSSMs is presented that value of magnetic flux density into inner and outer airgap is calculable and anticipatable. The magnetic flux density components due to permanent magnet and armature currents have been computed by analytical and numerical model which Analytical results are in good agreement with those obtained by FEM [18-30].

Appendix

$$n\left(a_{1n}r^{n-1} + a_{2n}r^{-n-1}\right) = S \tag{25}$$

$$-n\left(b_{1n}r^{n-1} + b_{2n}r^{-n-1}\right) = T \tag{26}$$

$$-n\left(a_{1n}r^{n-1} - a_{2n}r^{-n-1}\right) = F \tag{27}$$

$$-n\left(b_{1n}r^{n-1} - b_{2n}r^{-n-1}\right) = W \tag{28}$$

$$-\frac{m\pi}{\delta}c_{1jm}\left(R_{ri}^{\frac{m\pi}{\delta}-1} - R_{ryi}^{\frac{2m\pi}{\delta}} R_{ri}^{\frac{-m\pi}{\delta}-1}\right) = N \tag{29}$$

$$-\frac{m\pi}{\delta}c_{1jm}\left(R_{ri}^{\frac{m\pi}{\delta}-1} + R_{ryi}^{\frac{2m\pi}{\delta}} R_{ri}^{\frac{-m\pi}{\delta}-1}\right) = L \tag{30}$$

$$-\frac{\pi v}{\beta}\left(e_{1mj}\, \underline{r}^{\frac{v\pi}{\beta}-1} + e_{1mj}R_{pmi}^{\frac{2v\pi}{\beta}}\, r^{\frac{-v\pi}{\beta}-1}\right) = H \tag{31}$$

$$-\frac{\pi v}{\beta}\left(e_{1mj}\, \underline{r}^{\frac{v\pi}{\beta}-1} - e_{1mj}R_{pmi}^{\frac{2v\pi}{\beta}}\, r^{\frac{-v\pi}{\beta}-1}\right) = P \tag{32}$$

$$-\frac{u_0 M_j R_{pmi}}{r} + u_0 M_j = E \tag{33}$$

$$-\frac{k\pi}{\gamma}\left(\frac{u_0 J_{jk} r}{\left(\frac{k\pi}{\gamma}\right)^2-4}+d_{1kj} r^{\left(\frac{k\pi}{\gamma}\right)-1}+\left(\frac{2u_0 J_{jk}\frac{R_{yi}}{\left(\frac{k\pi}{\gamma}\right)^2-4}+\frac{k\pi}{\gamma}d_{1kj}R_{yi}^{\frac{k\pi}{\gamma}-1}}{\mathrm{k}\frac{\pi}{\gamma}R_{yi}^{\frac{-k\pi}{\gamma}-1}}\right)r^{\left(-\frac{k\pi}{\gamma}\right)-1}\right)=X \tag{34}$$

$$-\frac{1}{2}\frac{u_0 J_{j0} R_{yi}^{\ 2}}{r}+\frac{1}{2}u_0 J_{j0} r=R \tag{35}$$

$$-\left(2\frac{r u_0 J_k}{\left(\frac{k\pi}{\gamma}\right)-4}+\left(\frac{k\pi}{\gamma}\right)d_{1jk} r^{\frac{k\pi}{\gamma}-1}-\left(\frac{k\pi}{\gamma}\frac{\left(2\frac{u_0 J_k R_{yi}}{\left(\frac{k\pi}{\gamma}\right)^2-4}+\frac{k\pi}{\gamma}d_{1jk}R_{yi}^{\frac{k\pi}{\gamma}-1}\right)r^{-\frac{k\pi}{\gamma}-1}}{\frac{k\pi}{\gamma}R_{yi}^{\frac{-k\pi}{\gamma}-1}}\right)\right)=Y \tag{36}$$

$$\int_{\vartheta-\pi}^{\vartheta+\pi}(Fsin(n\theta)+Wcos(n\theta))\sin(n\theta)\,d\theta=\sum_{j=1}^{z}\int_{\vartheta+\alpha_j-\frac{\delta}{2}}^{\vartheta+\alpha_j+\frac{\delta}{2}}Ncos\left(\frac{m\pi}{\delta}\left(\theta-\alpha_j-\vartheta+\frac{\delta}{2}\right)\right)\sin(n\theta)\,d\theta \tag{37}$$

$$\int_{\vartheta-\pi}^{\vartheta+\pi}(Fsin(n\theta)+Wcos(n\theta))\cos(n\theta)\,d\theta=\sum_{j=1}^{z}\int_{\vartheta+\alpha_j-\frac{\delta}{2}}^{\vartheta+\alpha_j+\frac{\delta}{2}}Ncos\left(\frac{m\pi}{\delta}\left(\theta-\alpha_j-\vartheta+\frac{\delta}{2}\right)\right)\cos(n\theta)\,d\theta \tag{38}$$

$$\int_{-\pi}^{\pi}(Fsin(n\theta)+Wcos(n\theta))\sin(n\theta)\,d\theta=\sum_{j=1}^{x}\int_{\Gamma_j-\frac{\beta}{2}}^{\Gamma_j+\frac{\beta}{2}}\left(E+Pcos\left(\frac{\pi v}{\beta}\left(\theta-\Gamma_j+\frac{\beta}{2}\right)\right)\right)\sin(n\theta)d\theta+\sum_{j=1}^{y}\int_{\lambda_j-\frac{\delta}{2}}^{\lambda_j+\frac{\delta}{2}}\left(R+Ycos\left(\frac{k\pi}{\gamma}\left(\theta-\lambda_j+\frac{\delta}{2}\right)\right)\right)\sin(n\theta)d\theta \tag{39}$$

$$\int_{-\pi}^{\pi} (Fsin(n\theta) + Wcos(n\theta))\sin(n\theta)\, d\theta = \sum_{j=1}^{x} \int_{\Gamma_j - \frac{\beta}{2}}^{\Gamma_j + \frac{\beta}{2}} \left(E + Pcos\left(\frac{\pi v}{\beta}\left(\theta - \Gamma_j + \frac{\beta}{2}\right)\right)\right)\sin(n\theta)d\theta + \sum_{j=1}^{y} \int_{\lambda_j - \frac{\delta}{2}}^{\lambda_j + \frac{\delta}{2}} \left(R + Ycos\left(\frac{k\pi}{\gamma}\left(\theta - \lambda_j + \frac{\delta}{2}\right)\right)\right)\sin(n\theta)d\theta \tag{39}$$

$$\int_{-\pi}^{\pi} (Fsin(n\theta) + Wcos(n\theta))\cos(n\theta)\, d\theta = \sum_{j=1}^{x} \int_{\Gamma_j - \frac{\beta}{2}}^{\Gamma_j + \frac{\beta}{2}} \left(E + Pcos\left(\frac{\pi v}{\beta}\left(\theta - \Gamma_j + \frac{\beta}{2}\right)\right)\right)\cos(n\theta)d\theta + \sum_{j=1}^{y} \int_{\lambda_j - \frac{\delta}{2}}^{\lambda_j + \frac{\delta}{2}} \left(R + Ycos\left(\frac{k\pi}{\gamma}\left(\theta - \lambda_j + \frac{\delta}{2}\right)\right)\right)\cos(n\theta)d\theta \tag{40}$$

$$\int_{\vartheta + \alpha_j - \frac{\delta}{2}}^{\vartheta + \alpha_j + \frac{\delta}{2}} (Scos(n\theta) + Tsin(n\theta))\sin\left(\frac{m\pi}{\delta}\left(\theta - \alpha_j - \vartheta + \frac{\delta}{2}\right)\right) d\theta = \int_{\vartheta + \alpha_j - \frac{\delta}{2}}^{\vartheta + \alpha_j + \frac{\delta}{2}} Lsin^2\left(\frac{m\pi}{\delta}\left(\theta - \alpha_j - \vartheta + \frac{\delta}{2}\right)\right) d\theta \tag{41}$$

$$\int_{\Gamma[j] - \frac{\beta}{2}}^{\Gamma[j] + \frac{\beta}{2}} (S\cdot\cos(n\cdot\theta) + T\cdot\sin(n\cdot\theta)\cdot)\sin\left(\frac{\pi\cdot k\cdot}{\gamma}\left(\theta - \Gamma[j] + \frac{\beta}{2}\right)\right)d\theta - \int_{\Gamma[j] - \frac{\beta}{2}}^{\Gamma[j] + \frac{\beta}{2}} H \cdot\sin^2\left(\frac{\pi\cdot k\cdot}{\gamma}\left(\theta - \Gamma_j + \frac{\beta}{2}\right)\right)d\theta = 0 \tag{42}$$

$$\int_{\lambda_j - \frac{\gamma}{2}}^{\lambda_j + \frac{\gamma}{2}} (Scos(n\theta) + Tsin(n\theta))\sin\left(\frac{\pi k}{\gamma}\left(\theta - \lambda_j + \frac{\gamma}{2}\right)\right)d\theta = \int_{\lambda_j \frac{\gamma}{2}}^{\lambda_j + \frac{\gamma}{2}} Xsin^2\left(\frac{\pi k}{\gamma}\left(\theta - \lambda_j + \frac{\gamma}{2}\right)\right)d\theta \tag{43}$$

Competing Interests

This research is sponsored by [Bojnourd University] and may lead to development of products.

Funding

This research received no specific grant from any funding agency in the public, commercial, or not-for-profit sectors.

References

1. Li, Y., Bobba, D., & Sarlioglu, B. (2016). A novel 6/4 flux-switching permanent magnet machine designed for high-speed operations. IEEE Transactions on Magnetics, 52(8), 1-9.
2. Lee, C. H., Kirtley, J. L., & Angle, M. (2017). A partitioned-stator flux-switching permanent-magnet machine with mechanical flux adjusters for hybrid electric vehicles. IEEE Transactions on Magnetics, 53(11), 1-7.
3. Zhu, X., Hua, W., Wu, Z., Huang, W., Zhang, H., & Cheng, M. (2017). Analytical approach for cogging torque reduction in flux-switching permanent magnet machines based on magnetomotive force-permeance model. IEEE Transactions on Industrial Electronics, 65(3), 1965-1979.
4. Li, Y., Bobba, D., & Sarlioglu, B. (2016). Design and performance characterization of a novel low-pole dual-stator flux-switching permanent magnet machine for traction application. IEEE transactions on industry applications, 52(5), 4304-4314.
5. Hua, W., Zhang, H., Cheng, M., Meng, J., & Hou, C. (2016). An outer-rotor flux-switching permanent-magnet-machine with wedge-shaped magnets for in-wheel light traction. IEEE Transactions on Industrial Electronics, 64(1), 69-80.
6. Zhu, X., Xiang, Z., Zhang, C., Quan, L., Du, Y., & Gu, W. (2016). Co-reduction of torque ripple for outer rotor flux-switching PM motor using systematic multi-level design and control schemes. IEEE Transactions on Industrial Electronics, 64(2), 1102-1112.
7. Zhang, H., Hua, W., & Zhang, G. (2017). Analysis of back-EMF waveform of a novel outer-rotor-permanent-magnet flux-switching machine. IEEE Transactions on Magnetics, 53(6), 1-4.
8. Xiang, Z., Zhu, X., Quan, L., Du, Y., Zhang, C., & Fan, D. (2016). Multilevel design optimization and operation of a brushless double mechanical port flux-switching permanent-magnet motor. IEEE transactions on industrial electronics, 63(10), 6042-6054.
9. Cheng, M., Hua, W., Zhang, J., & Zhao, W. (2011). Overview of stator-permanent magnet brushless machines. IEEE Transactions on Industrial Electronics, 58(11), 5087-5101.
10. Wang, K., Zhu, Z. Q., Ombach, G., Koch, M., Zhang, S., & Xu, J. (2014). Electromagnetic performance of an 18-slot/10-pole fractional-slot surface-mounted permanent-magnet machine. IEEE Transactions on Industry Applications, 50(6), 3685-3696.
11. Dorrell, D. G., Knight, A. M., & Popescu, M. (2011). Performance improvement in high-performance brushless rare-earth magnet motors for hybrid vehicles by use of high flux-density steel. IEEE Transactions on Magnetics, 47(10), 3016-3019.
12. Cao, R., Mi, C., & Cheng, M. (2012). Quantitative comparison of flux-switching permanent-magnet motors with interior permanent magnet motor for EV, HEV, and PHEV applications. IEEE Transactions on magnetics, 48(8), 2374-2384.
13. Ooi, S., Morimoto, S., Sanada, M., & Inoue, Y. (2013). Performance evaluation of a high-power-density PMASynRM with ferrite magnets. IEEE Transactions on Industry Applications, 49(3), 1308-1315.
14. Bianchi, N., Fornasiero, E., Ferrari, M., & Castiello, M. (2015). Experimental comparison of PM-assisted synchronous reluctance motors. IEEE Transactions on Industry Applications, 52(1), 163-171.
15. Chai, F., Xia, J., Guo, B., & Cheng, S. (2008, June). Double-stator permanent magnet synchronous in-wheel motor for hybrid electric drive system. In 2008 14th Symposium on Electromagnetic Launch Technology (pp. 1-5). IEEE.
16. Hua, W., Zhang, G., & Cheng, M. (2015). Investigation and design of a high-power flux-switching permanent magnet machine for hybrid electric vehicles. IEEE Transactions on magnetics, 51(3), 1-5.
17. McFarland, J. D., Jahns, T. M., & EL-Refaie, A. M. (2015). Analysis of the torque production mechanism for flux-switching permanent-magnet machines. IEEE Transactions on Industry Applications, 51(4), 3041-3049.
18. Shao, L., Hua, W., & Cheng, M. (2015, October). A new 12/11-pole dual three-phase flux-switching permanent magnet machine. In 2015 18th International Conference on Electrical Machines and Systems (ICEMS) (pp. 1502-1507). IEEE.
19. Xiang, Z., Quan, L., Zhu, X., & Wang, L. (2015). A brushless double mechanical port permanent magnet motor for plug-in HEVs. IEEE Transactions on Magnetics, 51(11), 1-4.
20. Sikder, C., Husain, I., & Ouyang, W. (2015). Cogging torque reduction in flux-switching permanent-magnet machines by rotor pole shaping. IEEE Transactions on Industry Applications, 51(5), 3609-3619.
21. Dupas, A., Hlioui, S., Hoang, E., Gabsi, M., & Lecrivain, M. (2015). Investigation of a new topology of hybrid-excited flux-switching machine with static global winding: Experiments and modeling. IEEE Transactions on Industry Applications, 52(2), 1413-1421.
22. Li, S., Li, Y., & Sarlioglu, B. (2015). Partial irreversible demagnetization assessment of flux-switching permanent magnet machine using ferrite permanent magnet material. IEEE Transactions on Magnetics, 51(7), 1-9.
23. Zhang, G., Hua, W., & Cheng, M. (2016). Rediscovery of permanent magnet flux-switching machines applied in EV/HEVs: Summary of new topologies and control strategies. Chinese Journal of Electrical Engineering, 2(2), 31-42.
24. Cao, R., Jin, Y., Zhang, Y., & Cheng, M. (2016). A new double-sided HTS flux-switching linear motor with series magnet circuit. IEEE Transactions on Applied Superconductivity, 26(7), 1-5.
25. Du, Y., Zou, C., Zhu, X., Zhang, C., & Xiao, F. (2016). A full-pitched flux-switching permanent-magnet motor. IEEE Transactions on Applied Superconductivity, 26(4), 1-5.
26. Cao, R., Yuan, X., Jin, Y., & Zhang, Z. (2018). MW-class stator wound field flux-switching motor for semidirect

drive wind power generation system. IEEE Transactions on Industrial Electronics, 66(1), 795-805.
27. Gandhi, A., & Parsa, L. (2016). Double-rotor flux-switching permanent magnet machine with yokeless stator. IEEE transactions on energy conversion, 31(4), 1267-1277.
28. Jia, H., Wang, J., Cheng, M., Hua, W., Fang, C., & Ling, Z. (2016). Comparison study of electromagnetic performance of bearingless flux-switching permanent-magnet motors. IEEE Transactions on Applied Superconductivity, 26(4), 1-5.
29. Kim, D., Hwang, H., Bae, S., & Lee, C. (2016). Analysis and design of a double-stator flux-switching permanent magnet machine using ferrite magnet in hybrid electric vehicles. IEEE Transactions on Magnetics, 52(7), 1-4.
30. Li, H., & Zhu, H. (2016). Design of bearingless flux-switching permanent-magnet motor. IEEE Transactions on Applied Superconductivity, 26(4), 1-5.
31. Guo, T., Schofield, N., & Emadi, A. (2016). Double segmented rotor switched reluctance machine with shared stator back-iron for magnetic flux passage. IEEE Transactions on Energy Conversion, 31(4), 1278-1286.
32. Wang, Z., Xu, W., & Ye, C. (2016, November). In-wheel outer rotor flux switching permanent magnet machine with fractional-slot concentrated windings for electrical vehicles. In 2016 IEEE Conference on Electromagnetic Field Computation (CEFC) (pp. 1-1). IEEE.
33. Mo, L., Zhu, X., Zhang, T., Quan, L., Lu, Q., & Bai, X. (2018). Loss and efficiency of a flux-switching permanent-magnet double-rotor machine with high torque density. IEEE Transactions on Magnetics, 54(11), 1-5.
34. Yıldırız, E., Güleç, M., & Aydın, M. (2018). An innovative dual-rotor axial-gap flux-switching permanent-magnet machine topology with hybrid excitation. IEEE Transactions on Magnetics, 54(11), 1-5.
35. Zhou, L., Hua, W., & Cheng, M. (2017). Analysis and optimization of key dimensions of co-axial dual-mechanical-port flux-switching permanent magnet machines for fuel-based extended range electric vehicles. CES Transactions on Electrical Machines and Systems, 1(3), 292-299.
36. Xiang, Z., Quan, L., Zhu, X., Huang, J., & Fan, D. (2017). Investigation of optimal split ratio in brushless dual-rotor flux-switching permanent magnet machine considering power allocation. IEEE Transactions on Magnetics, 54(3), 1-4.
37. Xiang, Z., Zhu, X., Quan, L., Du, Y., Zhang, C., & Fan, D. (2016). Multilevel design optimization and operation of a brushless double mechanical port flux-switching permanent-magnet motor. IEEE transactions on industrial electronics, 63(10), 6042-6054.
38. Hua, W., Zhang, G., & Cheng, M. (2015). Investigation and design of a high-power flux-switching permanent magnet machine for hybrid electric vehicles. IEEE Transactions on magnetics, 51(3), 1-5.
39. Dai, M., Quan, L., Zhu, X., Xiang, Z., & Zhou, H. (2014, August). Design of a sandwiched flux switching permanent magnet machine with outer-rotor configuration. In 2014 IEEE Conference and Expo Transportation Electrification Asia-Pacific (ITEC Asia-Pacific) (pp. 1-5). IEEE.
40. Kim, J. H., Liu, M., Ding, H., & Sarlioglu, B. (2017, October). Comparison of dual structure axial flux-switching permanent magnet machines. In 2017 IEEE Energy Conversion Congress and Exposition (ECCE) (pp. 328-333). IEEE.
41. Boughrara, K., Lubin, T., & Ibtiouen, R. (2013). General subdomain model for predicting magnetic field in internal and external rotor multiphase flux-switching machines topologies. IEEE Transactions on Magnetics, 49(10), 5310-5325.
42. Gysen, B. L., Ilhan, E., Meessen, K. J., Paulides, J. J., & Lomonova, E. A. (2010). Modeling of flux switching permanent magnet machines with Fourier analysis. IEEE Transactions on Magnetics, 46(6), 1499-1502.
43. Yu, D., Yunyun, C., & Linlin, Y. (2017, August). Design and comparison of double-stator and conventional flux switched permanent magnet motor. In 2017 20th international conference on electrical machines and systems (ICEMS) (pp. 1-4). IEEE.
44. Yang, H., Lin, H., Li, Y., Wang, H., Fang, S., & Huang, Y. (2017). Analytical modeling of switched flux memory machine. IEEE Transactions on Magnetics, 54(3), 1-5.
45. Yang, H., Lin, H., Li, Y., Wang, H., Fang, S., & Huang, Y. (2017). Analytical modeling of switched flux memory machine. IEEE Transactions on Magnetics, 54(3), 1-5.
46. Shirzad, E., Pirouz, H. M., & Shirzad, M. T. (2023). Subdomain method for brushless double-rotor flux-switching permanent magnet machines with yokeless stator. Electrical Engineering, 1-11.
47. Shirzad, E., & taghi Shirzad, M. (2022). Multilevel Optimum Design of Double Rotor Brushless Flux-Switching Permanent Magnet Motor.
48. Shirzad, E. (2022). Fast-Response Method for E-core switched-flux permanent-magnet brushless machine with Outer Rotor to Predict Distribution of Flux density at No-Load.
49. Shirzad, E. (2023). Sub-Region Model for Flux-Switching Permanent Magnet Machine with Outer Rotor and Inner Rotor Distinctly to Calculate Cogging Torque, Electromagnetic Torque and Inductance (self and mutual).
50. Shirzad, E. (2023). Optimized Design by Genetic Algorithm for Flux Switching Brushless Permanent Magnet Machines with Two Ports from Perspective of Losses.